Downscaling of Spatial Irradiance Based on Cloud Advection using Transfer Functions

Joseph Ranalli
Penn State Hazleton
Hazleton, PA
jar339@psu.edu

Esther E.M. Peerlings
German Aerospace Center (DLR), Institute of Networked Energy Systems
Oldenburg, Germany
Esther.Peerlings@dlr.de

***Abstract*—Spatiotemporal aggregation of solar irradiance occurs when a spatially distributed receiver (e.g. a PV generation facility) collects variable, geographically distributed irradiance and reduces it to a single electrical generation output. Models of this phenomenon exist and are designed to take variability from a single point irradiance monitor and predict how that variability will be reduced by aggregation. We have applied these models in reverse to assess whether the same models can be used to predict the variability of a single point measurement given an aggregate irradiance time series as an input. Results for an advection-based model show that this approach leads to overprediction of the high frequency variability due to overprediction of the site-to-site correlation, even during highly correlated advection conditions. While some modifications to the cloud advection model improve its performance, the wavelet variability model better represents the site pair decorrelation and produces superior results in representing the disaggregated time series and variability metrics. Further work may be warranted to further improve upon these efforts and enable reliable, transfer function-based downscaling of irradiance data.**

***Index Terms*—variability, spatial aggregation, wavelet variability model, transfer function, downscaling**

I. Introduction

Spatiotemporal variability of solar irradiance and its characterization are well studied in the literature [1], [2]. It is important to have a good understanding of variability for both photovoltaic (PV) plant management and transmission grid operation, in order to anticipate and handle short term ramp events in power generation. One specific aspect of spatiotemporal variability that has been studied in the literature is modeling how variability of a single point sensor is reduced by the aggregation effect, since irradiance is actually received by a spatially distributed plant [3]–[5].

Variability in irradiance may result from several root phenomena. Variability induced by clouds occurs on a variety of timescales and due to its stochastic nature, may be more difficult to model and anticipate than other sources of variability. The Cloud Advection Model (CAM) of Ranalli et al. [5], [6] uses a transfer function to represent aggregation of irradiance during conditions when clouds pass over a plant without evolving in time. The CAM showed better performance than other models for representing spatial aggregation of irradiance during highly correlated, cloud advection dominated conditions. Its performance declined relative to other models, such as the wavelet variability model (WVM) [7], as larger plants with a higher degree of spatial decorrelation were considered [5].

In this study, we consider the possibility of performing the reverse aggregation operation: predicting the downscaled irradiance time series of a single point reference site based on an spatially aggregated irradiance input. In principle, the CAM's use of transfer functions to model the aggregation is an easily reversible process. This is similar to the work by Lave and Weekly who used an extrapolated transfer function to generate a high frequency irradiance time series from low resolution data [8]. The WVM can also be formulated for the reversed problem. We will consider both the CAM and the WVM here.

II. Models

In this section we will describe how both the CAM and the WVM were formulated to solve the reverse aggregation problem (disaggregation).

A. Cloud Advection Model

For a more detailed derivation of the CAM, readers may consult the original references [5], [6], but a summary is provided here. The CAM solves for the aggregation of a 1-D plant subject to advection of a frozen cloud field over its spatial extent. Irradiance at any given point within the spatial distribution is assumed to be represented by a delayed version of the irradiance at the reference site.

$$g(x,t) = g_{ref}(t - \frac{x}{V_c}) \tag{1}$$

The CAM utilizes a transfer function representation, which casts the reference site irradiance as an input and the aggregate plant irradiance as an output. Since the assumption of frozen clouds leads to a convolution of the irradiance and the plant as a representation of the aggregation, this transfer function can be shown to be equivalent to the Fourier transform of the plant's 1-D spatial distribution, d^*.

$$TF(f) = \mathcal{F}\left[d^*\left(\frac{x}{V_c}\right)\right] \tag{2}$$

The original formulation of the CAM transfer function considers the input to be the frequency representation of a

single site, $G_{ref}(f)$, and outputs the plant's aggregated output, $P(f)$. This is shown by Eq. 3

$$TF(f) = \frac{P(f)}{G_{ref}(f)} \tag{3}$$

Given the reversible nature of the transfer function, in this study, we compute the disaggregation by instead considering a plant's aggregated time signal to be the input. We compute the transfer function of the distributed plant in the same way as the original formulation, but predict the time series of a single site as an output. This is done mathematically by solving Eq. 3 for $G_{ref}(f)$ and performing the inverse Fourier transform to yield the single point irradiance time series, $g_{ref}(t)$. This leads to division by the modeled plant transfer function. The single site irradiance can then be converted to clear sky index, k_c, by dividing by clear sky irradiance.

B. Wavelet Variability Model

Because each of the factors of the WVM is considered to be stationary in time, it can essentially be considered to be similar to a transfer function, despite not following an explicit transfer function methodology. The WVM [3] splits a signal into individual wavelet modes and scales them down by use of a variability reduction factor (VR). To calculate VR, the WVM relies on the correlations between individual site pairs, which in turn depend on the wavelet mode's time scale, the cloud speed and the site pair separation distance [7], as in Eq. 4.

$$\rho = \exp\left(-\frac{L}{(V_c/2)\Delta t}\right) \tag{4}$$

The VR is defined as the average of these correlations for all possible site pairs.

$$VR = \frac{N^2}{\sum \rho_i} \tag{5}$$

In the original WVM formulation, each wavelet mode is scaled down by dividing by the square root of VR to give greater reduction of variability at higher frequencies.

$$w_P(t) = \frac{w_{ref}(t)}{\sqrt{VR}} \tag{6}$$

In order to reverse this process, we rearrange Eq. 6 such that instead of dividing by $\sqrt{VR}$, we multiply, thus solving for a reference site's mode shape, w_{ref}, as a function of the aggregate plant mode, w_P. As in the original case, summing over all the reference wavelet modes yields the prediction of the reference site's clear sky index index time signal [3].

III. Results and Discussion

We have performed the downscaling calculation on a real spatially distributed dataset to test the efficacy of these approaches. To match the initial use of the CAM, we chose a subset of 9 sites from the HOPE-Melpitz measurement campaign [9] aligned in an approximately linear direction (i.e. a 1-D plant distribution). We selected a one hour window during which strong cloud advection was observed. We used the output of the aggregated linear subset of sites as an input to the models and compared the results for a centrally located single reference site. The central position of the reference is important for the WVM, which does not intrinsically account for time lag in the signals. Details of the 9 sites chosen and their location within the site are provided in [6].

A. Metrics

To quantify the performance of the two models at representing the downscaled time series, we considered several metrics, particularly focused on those related to variability. We computed the power spectral density (PSD) of the known reference vs. modeled time series and compared visually using plots. We computed the root mean square error (RMSE) for the clear sky index time series compared between the single site reference and the model output. We also used the common variability metrics [2] of variability index, variability score and standard deviation of ramp rates .

Variability Index (VI) is defined as the ratio between the path length of the actual irradiance curve and the clear sky irradiance curve [10]. In computing the path length, it measures a change in irradiance or ramp rate, RR, over a time increment, Δt, which is measured in minutes. For this study, VI was only computed for a Δt equal to the sampling period of the data of 1 second.

$$VI = \frac{\sum \sqrt{RR^2 + \Delta t^2}}{\sum \sqrt{RR_{clear}^2 + \Delta t^2}} \tag{7}$$

Variability Score (VS) is a measure based on the maximum value of the product of a ramp rate magnitude, RR_i, and the probability of occurrence of said ramp rate. The variability score is normalized by the STC irradiance (1000 W/m^2) and multiplied by 100 for scaling [11]. In the results we compute VS using Δt equal to 5 seconds, 30 seconds and 60 seconds. Temporal averaging was used to produce time series with the appropriate resolution to compute ramp rates at these intervals.

$$VS_{\Delta t} = 100 \times max\left[RR_i \times P\left(|RR| > RR_i\right)\right] \tag{8}$$

Finally, the standard deviation of clear sky index ramps, $\sigma\left(\Delta k_{c_{\Delta t}}\right)$, was computed for variable Δt. For the purposes of computing this metric, a raw difference (i.e. no averaging) was used to compute the clear sky index ramps.

B. Results

The predicted aggregation transfer function for the CAM based on the 9 site plant is shown in Fig. 1. The transfer function is an overall low-pass filter with some dynamics that allow some bands of high frequency content to pass. Dividing by this transfer function will therefore result in an increase in the magnitude of the high frequencies, while the low frequencies will remain approximately constant.

The results of the inverse (disaggregation) transformation for both time series and standard deviation of ramp rates are shown in Fig. 2. The result from the CAM shows a significant

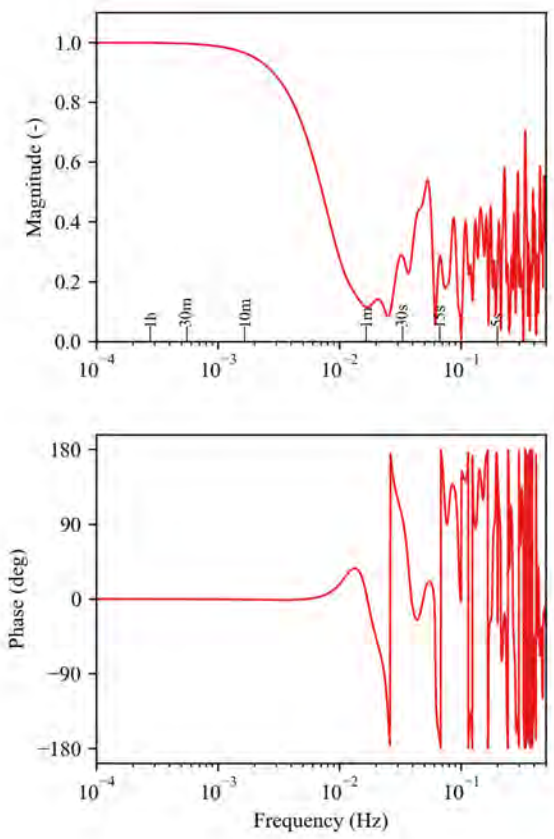

Fig. 1. Predicted transfer function for the plant configuration during the 1 hour window studied here. Several time scales corresponding to the frequencies are labelled.

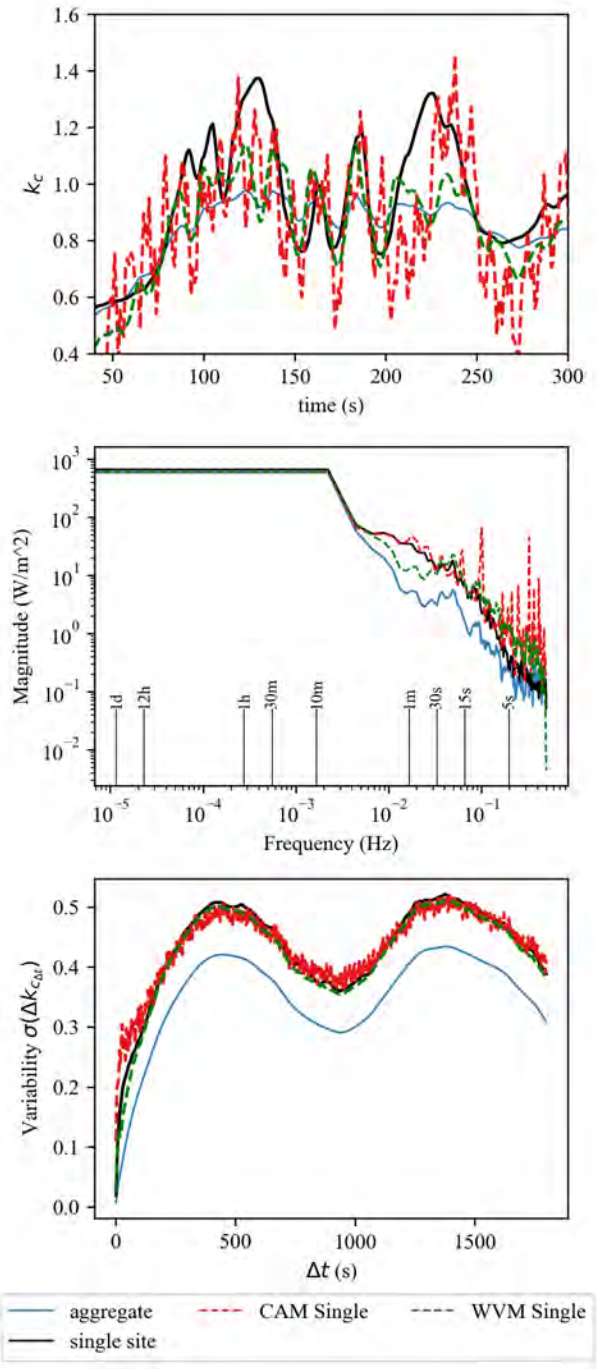

Fig. 2. Disaggregation calculation time series, power spectrum and variability for 9 sites disaggregated to a single reference. Spectra are smoothed using 8 averages with a Hanning window and 50% overlap.

degree of high frequency content. This is visible both in the time series, and the variability, which is significantly overpredicted for small Δt. The WVM exhibits a more realistic time series than the CAM. In part, we attribute this difference to the nature of the models. Because the CAM assumes perfect correlation between sites at all frequencies, high frequency pass dynamics are present as seen in Fig. 1. When dividing by the transfer function, this results in substantial amplification of the high frequencies, as seen in the power spectrum. Because the WVM is based upon decorrelation between sites, and thus exclusively suppresses high frequency content, it appears to do a better job of creating a realistic time series. This is also reflected by the WVM's much closer match to the target value on most of the variability metrics as seen in Table I. The WVM performs reasonably well at predicting the time series and the variability according to these metrics. At high frequency (i.e. the VI and the VS for a 5 second Δt), the CAM seriously overpredicts the variability. The CAM's performance improves at lower frequencies (i.e. VS for 30 second and 60 second time scales).

One interesting factor revealed in the PSD plot in Fig. 2 is that the CAM matches the PSD better in the band from roughly

TABLE I
VARIABILITY METRICS FOR MODELING THE SPATIAL DISAGGREGATION.

Metric	Agg.	Target	CAM	WVM
RMSE	-	-	0.184	0.133
VI	103.6	274.6	2365.8	385.2
VS5	0.37	1.01	3.40	1.07
VS30	1.38	2.52	2.75	2.01
VS60	2.53	3.31	2.99	3.46

TABLE II
VARIABILITY METRICS FOR MODIFIED CAM. TARGET AND WVM RESULTS ARE UNCHANGED.

Metric	Agg.	Target	CAM	WVM
RMSE	-	-	0.157	0.133
VI	103.6	274.6	496.9	385.2
VS5	0.37	1.01	1.63	1.07
VS30	1.38	2.52	2.72	2.01
VS60	2.53	3.31	3.07	3.46

0.01-0.04 Hz. This corresponds to the low magnitude band in the CAM transfer function following the initial frequency cutoff (see Fig. 1). This reduction in magnitude is associated with spatial interference phenomena and only occurs when considering high site-to-site coherence due to cloud advection [5], [6], which is not described by the WVM formulation.

We demonstrate one possible improvement on the CAM disaggregation calculation by limiting amplification of high frequency portions of the input, where we would expect site pair correlation to decline. The CAM's broadly elevated power spectrum magnitude beyond about 0.2 Hz contributes to the undesirable oscillating signal in the time series. So for these high frequency cases, we considered replacing the predicted disaggregated power spectrum values with those of the aggregate power spectrum (i.e. the input) based on a threshold on the aggregate power spectrum magnitude (magnitude less than 0.4 in this demonstration). This attempts to correct for the fact that uncorrelated parts of the signal are present at high frequencies in the power spectrum, and the assumption of correlation (coherence) inherent to the CAM transfer function approach is violated. The results of this simple correction are shown in Fig. 3. As is evident, this correction removes the high frequency oscillations and creates a somewhat more realistic time series. The PSD is also more realistic, but the CAM's standard deviation variability metric is reduced below the target values, except at very low frequencies, where variability is overpredicted. The WVM results remain the same as for the previous comparison. The CAM results at high frequency are improved substantially by suppressing the high frequency, uncorrelated content, as shown by the metrics in Table II, though the CAM continues to consistently overpredict when compared to the target values. We observe that the performance of the WVM remains superior to the modified CAM for most metrics.

To further investigate these results, we considered the probability density of the clear sky index ramp rates during this one hour window at the 5, 30 and 60 second ramp intervals, as shown in Fig. 4. As observed by other investigators [12], the peak probability occurs for a zero ramp event and falls off for increasing ramp magnitudes. Comparing the actual input and output measurement data (i.e. real aggregate vs. single site) we observe that at the 5 secont time scale, the large ramps are significantly suppressed by the aggregate case, but are present in the single site measurement. When comparing with the models, the WVM performs better than the CAM. The WVM slightly overpredicts the frequency of moderate

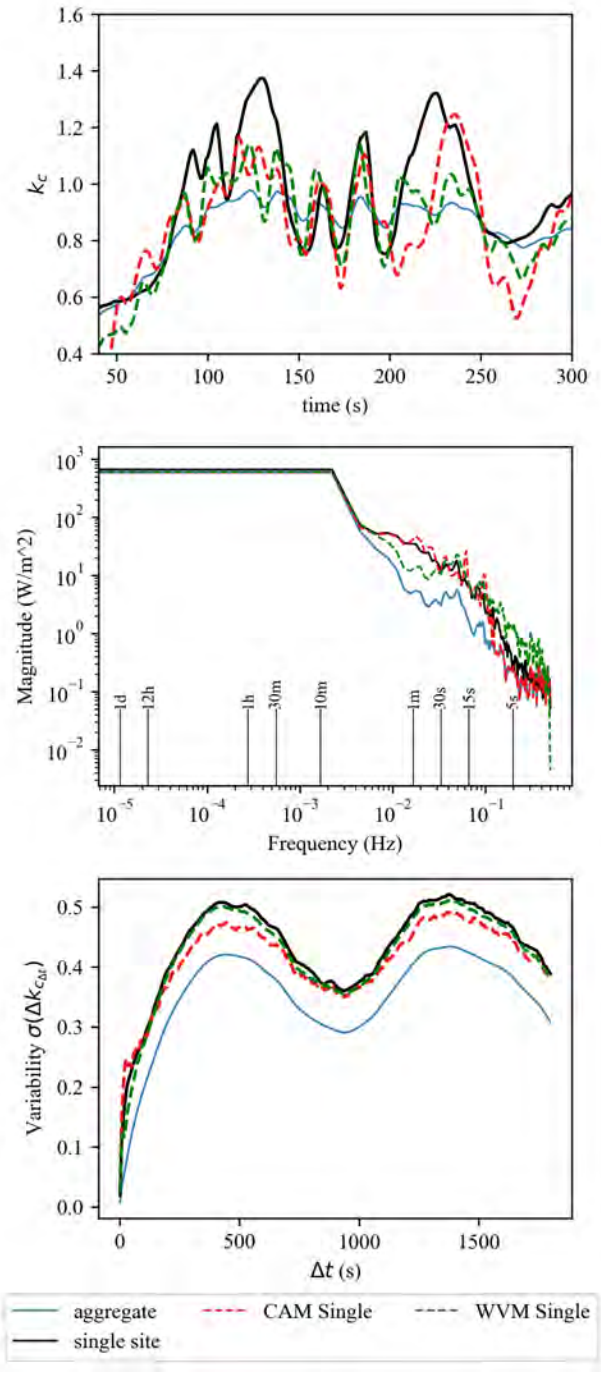

Fig. 3. Disaggregation calculation time series, power spectrum and variability for 9 sites disaggregated to a single reference, with the low-power-spectrum-magnitude correction applied to the CAM. Spectra are smoothed using 8 averages with a Hanning window and 50% overlap.

ramp events, while providing a more accurate prediction of the frequency of the largest ramp events. Despite reducing its high frequency power spectral density to match the aggregate case, the modified CAM still overpredicts the frequency of all magnitudes of ramp events at this 5 second timescale, leading to underprediction of frequency of the zero ramp case. When considering 30 and 60 second ramp rates (i.e. lower frequencies), we see that the difference between the aggregated and single site distributions is not as significant. We also see that the results of the two models are more closely comparable, as was evidenced by the numerical metric data discussed previously.

One possible interpretation of the superiority of the WVM results at high frequency follows from understanding the different formulations between the two models. By assuming advection of frozen clouds, the CAM represents perfect correlation between all site pairs (when accounting for delay). The CAM model's predicted transfer function shape can be thought of as arising from interference patterns that occur as a result of the delayed irradiance reaching different locations within the plant at different instants. That is, at certain frequencies, these delayed oscillations will occur in- or out-of-phase, and will constructively or destructively interfere when integrating over the plant. However, as described by Ranalli and Peerlings [5], the coherence in the real data falls off significantly with increasing frequency. This results from the presence of uncorrelated high frequency components of the signal, which can be interpreted to show that at their smallest length scales, clouds can not be assumed to advect across the plant in a frozen manner. When performing the inverse transform operation (dividing by the transfer function), these high frequencies are not as highly correlated as the CAM assumes, and thus they are amplified in an unrealistic manner. The WVM, which assumes a degree of decorrelation between sites (particularly so at high frequencies) is more resilient to this problem and is not as susceptible to the artificial magnificiation of uncorrelated high frequency content.

Given the results for the 1-D plant configuration, we also investigated performance for a somewhat more general plant distribution. We applied the WVM to four separate one-hour periods using the entire 2-D field from the HOPE-Melpitz campaign as the aggregate plant. Results for this calculation are shown in Fig. 5. Identification of the cloud motion vectors for these cases used a form of the cross spectral analysis method described by Jamaly and Kleissl [13]. This method computes a cloud motion vector by varying the vector's direction in order to minimize the variance in the distribution of all pairwise velocities. Each pairwise velocity is computed using site pair separation and the lag at which maximum cross correlation in the clear sky index time series occurs. Once the vector is identified, the median of the velocity distribution is used as the cloud speed. We adopted the quality control of Jamaly and Kleissl [13] for this process, but also added a low limit on clear sky index to eliminate overcast conditions. Full details of the cloud motion vector identification method are provided in [5].

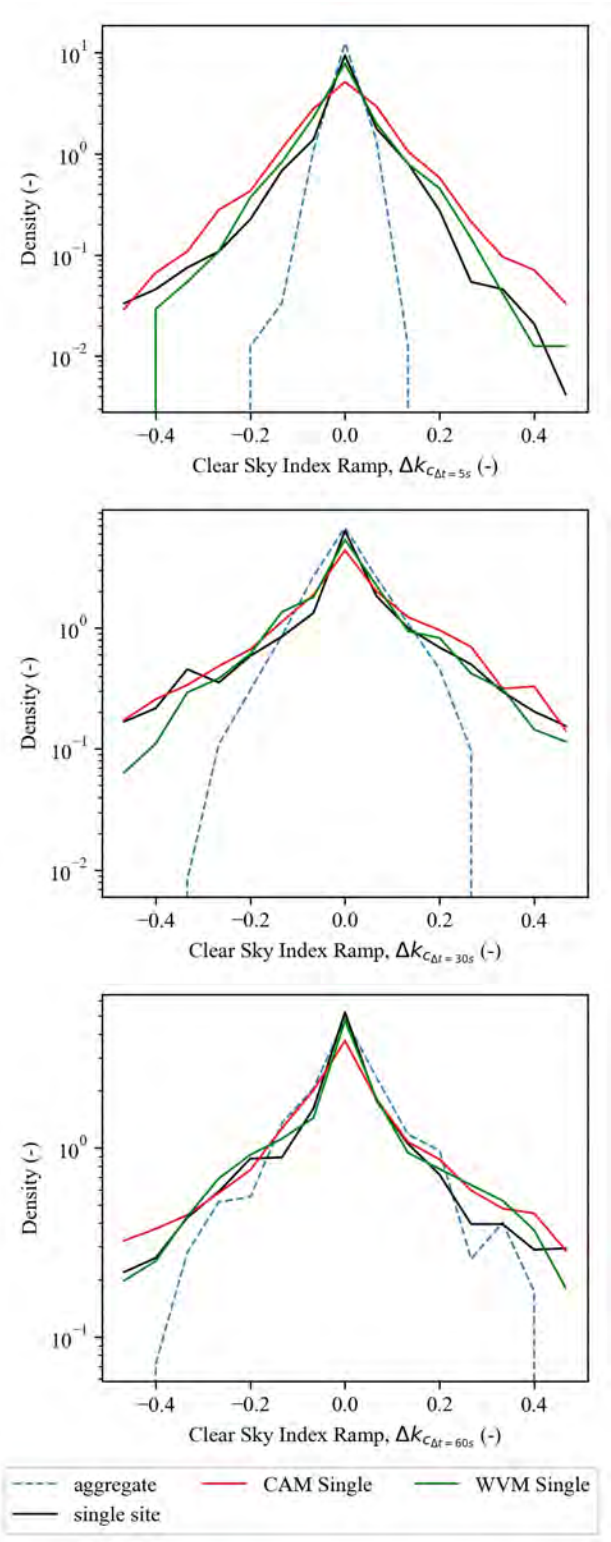

Fig. 4. Probability density of the clear sky index ramps for the modified CAM and the WVM. From top to bottom, the three separate plots use ramp rate increments of Δt = 5 s, Δt = 30 s and Δt = 60 s.

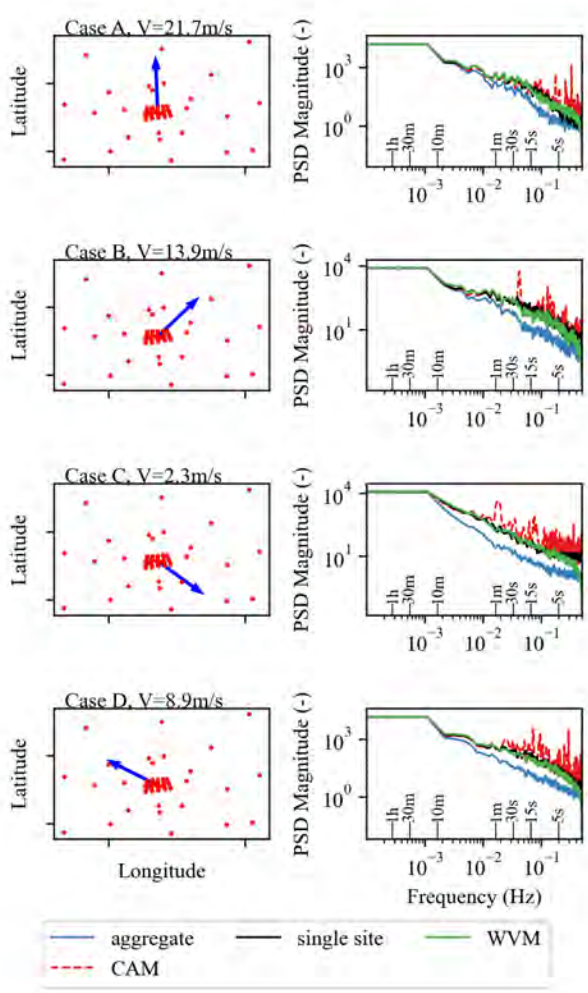

Fig. 5. Comparison of the disaggregation for four separate one hour periods with variable cloud speed and direction. Input measurement was based on the entire set of site measurements from the HOPE-Melpitz campaign. Left column shows the plant configuration along with the cloud motion vector in blue. Right column shows the power spectral density.

The WVM does a reasonable job at representing the disaggregated power spectrum for the variable cloud motion speeds and directions investigated. While the CAM also predicts the rough overall shape of the power spectrum, it substantially overpredicts the variability, particularly at high frequency[1]. Comparisons of the accuracy of the models based on the variability metrics considered previously are given in Table III. As before, the CAM significantly overpredicts the variability for metrics that capture high frequency behavior, but produces reasonable results for lower frequencies. The WVM seems to provide a more reasonable representation of the variability in the time series for the metrics.

[1]Use of the modified CAM described previously would require manual tuning of the magnitude threshold, thus the results shown here are for the unmodified CAM.

IV. Conclusion

While this demonstration does show the possibility of using transfer functions derived from the cloud advection model (CAM) for disaggregation, results indicate that the technique leads to some degree of undesirable amplification of uncorrelated high frequency content, due to a failed assumption of site-pair correlation at high frequencies. The wavelet variability model (WVM) can also be modified to compute the spatial disaggregation operation and was applied to produce a prediction of a disaggregated time series. The WVM's basis on decorrelation between site-pairs helps to suppress the amplification of uncorrelated parts of the signal that was observed for the CAM. The results for the WVM on several variability metrics were uniformly superior to those for the CAM. This is true even for the 1-D case where coherent advection would be expected to be a dominant factor, and where the CAM showed superior performance in previous studies dealing with the "ordinary" aggregation modeling approach. The WVM's superior performance was even more evident when considering plants with a larger cross-wind geographic distribution.

One important limitation to both of these approaches as a downscaling methodology is that the results produced are deterministic in nature. That is, for a given plant and reference position within it, the disaggregated time series will always be the same. It may be possible to marry one of these approaches with other spatiotemporal variability downscaling techniques that generate statistical representations of the time series in order to incorporate a non-deterministic variability and to form a more complete model.

We believe that this study demonstrates the possibility of using a reversed form of spatial aggregation models (in particular the WVM) to disaggregate (that is, spatially downscale) irradiance data from a spatial aggregate measurement to a single site reference. That said, the validations performed in this study were limited to one hour windows within a point-cloud measurement data set. Further work remains necessary to validate this approach for more generalized cases, including continuously distributed plants, and to identify potential pitfalls that may not have been observed in this preliminary study.

V. Acknowledgment

J.R. acknowledges financial support by Penn State Engineering Technology and Commonwealth Engineering and Penn State Hazleton, and appreciates the support of the Carl von Ossietzky University of Oldenburg and the DLR Institute for Networked Energy Systems who hosted his visiting scientist appointment. Part of this work was supported by the Federal Ministry of Economic Affairs and Energy on the basis of a decision by the German Bundestag (project HyForPV, grant 0350032B).

References

[1] R. Perez, M. David, T. E. Hoff, M. Jamaly, S. Kivalov, J. Kleissl, P. Lauret, and M. Perez, "Spatial and Temporal Variability of Solar Energy," *Foundations and Trends in Renewable*

TABLE III
VARIABILITY METRICS FOR WVM FOR THE CASES SHOWN IN IN FIG. 5.

Case	A				B				C				D			
Metric	Agg.	Target	CAM	WVM	Agg.	Target	CAM	WVM	Agg.	Target	CAM	WVM	Agg.	Target	CAM	WVM
RMSE	-	-	0.115	0.048	-	-	0.334	0.072	-	-	0.401	0.167	-	-	0.363	0.095
VI	112.9	303.3	3871.2	344.0	33.7	125.5	1018.9	132.9	33.1	109.0	1161.3	154.1	91.7	287.1	8415.3	450.9
VS5	0.30	0.71	1.14	0.76	0.17	0.52	5.66	0.51	0.12	0.31	4.31	0.64	0.16	0.61	6.92	0.69
VS30	1.31	2.10	1.85	2.13	0.69	1.11	1.92	1.28	0.52	1.49	7.44	1.82	0.57	0.96	1.58	1.12
VS60	1.81	1.98	1.98	2.50	1.08	1.48	1.66	1.74	0.99	2.26	2.71	2.66	0.91	1.57	2.10	1.85

Energy, vol. 1, no. 1, pp. 1–44, Jul. 2016. [Online]. Available: https://www.nowpublishers.com/article/Details/REN-006

[2] G. M. Lohmann, "Irradiance Variability Quantification and Small-Scale Averaging in Space and Time: A Short Review," *Atmosphere*, vol. 9, no. 7, p. 264, Jul. 2018. [Online]. Available: https://doaj.org

[3] M. Lave, J. Kleissl, and J. S. Stein, "A Wavelet-Based Variability Model (WVM) for Solar PV Power Plants," *IEEE Transactions on Sustainable Energy*, vol. 4, no. 2, pp. 501–509, Apr. 2013.

[4] J. Marcos, I. d. l. Parra, M. Garcia, and L. Marroyo, "Simulating the variability of dispersed large PV plants," *Progress in Photovoltaics: Research and Applications*, vol. 24, no. 5, pp. 680–691, 2016. [Online]. Available: https://onlinelibrary.wiley.com/doi/abs/10.1002/pip.2719

[5] J. Ranalli and E. E. Peerlings, "Cloud advection model of solar irradiance smoothing by spatial aggregation," *Journal of Renewable and Sustainable Energy*, 2021 (in press).

[6] J. Ranalli, E. E. Peerlings, and T. Schmidt, "Cloud Advection and Spatial Variability of Solar Irradiance." Virtual: IEEE, Jun. 2020, p. 8.

[7] M. Lave and J. Kleissl, "Cloud speed impact on solar variability scaling – Application to the wavelet variability model," *Solar Energy*, vol. 91, pp. 11–21, May 2013. [Online]. Available: http://www.sciencedirect.com/science/article/pii/S0038092X13000406

[8] M. Lave and A. Weekley, "Comparison of High-Frequency Solar Irradiance: Ground Measured vs. Satellite-Derived," Piscataway, NJ: Institute of Electrical and Electronics Engineers (IEEE), Tech. Rep. NREL/CP-6A20-67951, Nov. 2016. [Online]. Available: https://www.osti.gov/biblio/1343679-comparison-high-frequency-solar-irradiance-ground-measured-vs-satellite-derived

[9] A. Macke, P. Seifert, H. Baars, C. Barthlott, C. Beekmans, A. Behrendt, B. Bohn, M. Brueck, J. Bühl, S. Crewell, T. Damian, H. Deneke, S. Düsing, A. Foth, P. D. Girolamo, E. Hammann, R. Heinze, A. Hirsikko, J. Kalisch, N. Kalthoff, S. Kinne, M. Kohler, U. Löhnert, B. L. Madhavan, V. Maurer, S. K. Muppa, J. Schween, I. Serikov, H. Siebert, C. Simmer, F. Späth, S. Steinke, K. Träumner, S. Trömel, B. Wehner, A. Wieser, V. Wulfmeyer, and X. Xie, "The HD(CP)^2 Observational Prototype Experiment (HOPE) – an overview," *Atmospheric Chemistry and Physics*, vol. 17, no. 7, pp. 4887–4914, Apr. 2017. [Online]. Available: https://www.atmos-chem-phys.net/17/4887/2017/acp-17-4887-2017-discussion.html

[10] J. S. Stein, C. W. Hansen, and M. J. Reno, "The Variability Index: A New and Novel Metric for Quantifying Irradiance and PV Output Variability," in *Proceedings of the World Renewable Energy Forum*, Denver, CO, May 2012, pp. 13–17.

[11] M. Lave, M. J. Reno, and R. J. Broderick, "Characterizing local high-frequency solar variability and its impact to distribution studies," *Solar Energy*, vol. 118, pp. 327–337, 2015.

[12] G. M. Lohmann and A. H. Monahan, "Effects of temporal averaging on short-term irradiance variability under mixed sky conditions," *Atmospheric Measurement Techniques*, vol. 11, no. 5, pp. 3131–3144, May 2018. [Online]. Available: https://www.atmos-meas-tech.net/11/3131/2018/

[13] M. Jamaly and J. Kleissl, "Robust cloud motion estimation by spatio-temporal correlation analysis of irradiance data," *Solar Energy*, vol. 159, pp. 306–317, Jan. 2018. [Online]. Available: http://www.sciencedirect.com/science/article/pii/S0038092X17309556